Analyst

PAPER

View Article Online
View Journal | View Issue

Cite this: *Analyst*, 2019, **144**, 6283

Post-imprinting modification based on multilevel mesoporous silica for highly sensitive molecularly imprinted fluorescent sensors†

Hongzhi Lu,[a] Di Wei,[b] Rongkun Zheng[b] and Shoufang Xu *[b]

Received 7th August 2019,
Accepted 21st September 2019

DOI: 10.1039/c9an01503e

rsc.li/analyst

When molecularly imprinted fluorescent polymers (MIFPs) are prepared by the doping method (d-MIFPs), the fluorescent nanoparticles are quenched and passivated during the polymerization and elution process, and their detection sensitivity would be reduced. In this study, to overcome this drawback, MIFPs were synthesized by post-imprinting modification based on multilevel mesoporous structured silica. Briefly, multilevel mesoporous-structured BPA-imprinted polymers (MIPs) were prepared at first, and then, CdTe quantum dots were anchored onto the large pores of the MIPs to form p-MIFPs. Due to the well-maintained fluorescence intensity and low background, the sensitivity of the p-MIFPs was two orders of magnitude higher than that of the d-MIFPs. The $F_0/F - 1$ of p-MIFPs was linear with BPA in the range of 0.005 to 4.0 μM with an LOD of 0.57 nM. Furthermore, post-imprinting modification was adopted to achieve ratiometric fluorescent MIPs (p-r-MIFPs) by simultaneously anchoring carbon dots and quantum dots onto the MIPs. The p-MIFPs and p-r-MIFPs were successfully applied to determine BPA in water samples with average recoveries ranging from 96.4% to 102.0% and an RSD below 4.1%. The results prove that post-imprinting modification is an effective method to construct MIFPs with conspicuous sensitivity, and multilevel mesoporous silica is an ideal matrix for the post-imprinting modification.

Introduction

Molecular imprinting technique has proven to be a significant tool in the analytical area because it can be used to construct recognition sites that specifically match target molecules and meet the requirements of high selectivity for analytical detection.[1–6] Fluorescence technology has also been receiving enormous attention as a powerful detection tool in the sensing field because of its high sensitivity and simplicity.[7] Fluorescent sensors based on the molecular imprinting technique have been designed for the detection of organic compounds,[8,9] metal ions,[10] and proteins,[11] which have been thoroughly reviewed by Chen's groups.[12] Fluorescent nanoparticles, such as quantum dots (QDs),[13] carbon dots (CDs),[14] and gold nanoclusters,[15] exhibit the advantages of simple preparation, easy surface modification, and stability and are thus widely used in the preparation of molecularly imprinted fluorescent polymers (MIFPs). Generally, fluorescent nanoparticles are doped into the polymerization solution and then coated inside the polymer after the polymerization process. During the subsequent template elution process, the fluorescent nanoparticles are subjected to the washing solution for a long time, such that their fluorescence intensity is greatly reduced and the detection sensitivity of the MIFP is severely reduced. Thus, to improve the detection sensitivity and maintain the fluorescence intensity, the fluorescent nanoparticles can be introduced by post-imprinting modification. Specifically, MIPs are first prepared by a polymerization and template elution two-step operation, and then, the fluorescent nanoparticles are anchored onto the MIPs by chemical bonds. In the post-imprinting modification strategy, the fluorescent nanoparticles do not experience the long elution process, and their fluorescence intensity can be well maintained.

The morphology of MIPs plays a crucial role in the post-imprinting modification process. Spherical or bulk MIPs are unsuitable for the post-imprinting process because fluorescent nanoparticles can be bonded to only the surface of the MIPs and are thus difficult to be anchored inside the MIPs[16] due to their big particle size. The recognition sites inside the polymer are far from the fluorescent nanoparticles, and the conversion from molecular recognition to fluorescence signal output will be blocked. Mesoporous silica is widely used as an imprinting matrix because its large specific surface area is beneficial for mass transfer.[17] The diameter of fluorescent nanoparticles is generally about 2–3 nm, and the pores in the mesoporous

[a]*School of Chemistry and Chemical Engineering, Linyi University, Linyi 276005, China*
[b]*School of Materials Science and Engineering, Linyi University, Linyi 276005, China. E-mail: shfxu1981@163.com*

† Electronic supplementary information (ESI) available: Fig. S1–S7 and Table S1. See DOI: 10.1039/c9an01503e

silica are also about 2–3 nm. Thus, the introduction of fluorescent nanoparticles may block the mesopores and reduce the mass transfer efficiency, which is also adverse to post-imprinting modification. It is expected that the imprinting sites and mass transfer efficiency will be well-kept after the introduction of fluorescent nanoparticles. Therefore, multi-level mesoporous silica has attracted our attention.

Multi-level mesoporous silica belongs to the third-generation silica materials.[18] Two or more pore structures co-exist in the multi-level mesoporous silica. A variety of multi-level mesoporous silica with different morphologies, such as hollow mesoporous spheres, hollow spheres with multiple porous shells and radially porous spheres, can be prepared by regulation of the polymerization method. Radially porous silica spheres have two types of pore structures. One is mesopores with a diameter in the range of 2–3 nm, and the other is large pores with a diameter of serval tens nanometer. Radially porous silica is an ideal matrix for post imprinting modification. Its mesopores of about 2–3 nm guarantee a large surface area and facilitate the mass transfer. Its large pores provide sufficient space for anchoring fluorescent nanoparticles to ensure that the introduction of fluorescent nanoparticles does not decrease the adsorption capacity.

Bisphenol A (BPA), a phenolic environmental estrogen, can cause estrogenic endocrine disruption and promote tumor progression. Simultaneously, BPA is an important monomer for many plastics such as epoxy resin and polycarbonate. Because of its widespread use in numerous products, BPA enters surface water from effluent discharge during its manufacture, use, and from waste landfill sites worldwide. Thus, the measurement of BPA concentrations in water is important for evaluating compliance with water quality standards or environmental risk levels of this harmful compound in the environment.

In this work, as a proof of concept, BPA-imprinted fluorescent polymers were prepared based on multi-level mesoporous silica *via* the post-imprinting modification strategy. The whole preparation process included polymerization-template elution-fluorescent nanoparticle anchoring in three steps. Firstly, multi-level mesoporous silica was prepared *via* the water–ethanol–ethyl ether co-solvent method. Then the templates were eluted by acid ethanol. Finally, QDs were bonded to the multi-level mesoporous silica by condensation reaction between their carboxyl group and amino group. The as-prepared p-MIFPs exhibited good fluorescence properties and high sensitivity. Furthermore, to verify the application of the post-imprinting modification strategy in the construction of ratiometric fluorescent MIPs, QDs and CDs were simultaneously bonded to multi-level mesoporous silica, and a ratiometric fluorescent probe was constructed to realize the visual detection of BPA. p-MIFPs enjoy improved sensitivity over the MIFPs prepared by the doping method (d-MIFPs) due to the following reasons. First and most importantly, p-MIFPs have higher fluorescence intensity and lower background. Secondly, the QDs are uniformly distributed in p-MIFPs. Thirdly, acidic solvent can be used for elution, and thus the template elution is more thorough. Post-imprinting modification is an effective method to construct MIFPs, and multilevel mesoporous silica is an ideal matrix for post-imprinting modification. To the best of our knowledge, multilevel mesoporous-structured MIFPs are proposed herein for the first time by post-imprinting modification strategy based on multilevel mesoporous structured silica. The proposed method enriches the preparation method of MIFPs.

Experimental

Materials and apparatus

Citric acid, ethylenediamine, thioglycolic acid (TGA), bisphenol A (BPA), estradiol, phenol and cholesterol were purchased from Tianjin Reagent Plant (Tianjin, China). Cetyltrimethylammonium bromide (CTAB), aqueous ammonia, ethanol, ethyl ether, 3-aminopropyl triethoxy silane (APTES), tetraethoxysilane (TEOS) and *N*-hydroxysuccinimide (NHS) were obtained from Beijing Chemical Reagent Co.

Fluorescence spectra were recorded using an F-7000 spectrofluorometer (Hitachi). Morphology and particle size were characterized by transmission electron microscopy (TEM, JEM-2100F) and scanning electron microscopy (SEM, Hitachi S-4800 FE-SEM), respectively. A Micromeritics ASAP 2020 Sorptometer (Micromeritics, ASAP 2020, USA) was used for the determination of the BET surface area. An FT-IR spectrometer (Thermo Nicolet Corporation, USA) was employed to examine the infrared spectra.

Synthesis of carboxylic group-modified QDs and CDs

Carboxyl group-modified CdTe QDs were prepared using TGA as a stabilizer according to our previous work.[19] Carboxylic group-modified CDs were prepared using citric acid and ethylenediamine as precursors according to previous work.[20]

Synthesis of BPA-imprinted multilevel mesoporous silica

Multilevel mesoporous silica was prepared *via* the co-solvent method using CTAB as the surfactant, according to the previously reported method.[16] BPA-imprinted multilevel mesoporous silica (MIPs) was prepared based on the multilevel mesoporous silica with minor modification. Typically, 0.5 g CTAB was dissolved in an emulsion system composed of 70 mL of H_2O, 0.8 mL of aqueous ammonia, 20 mL of ethyl ether, and 10 mL of ethanol, followed by vigorously stirring for 0.5 h. Then a mixture of 2.5 mL of TEOS, 200 μL of APTES, 45.6 mg BPA was quickly dripped into the above mixture. The resulting mixture was vigorously stirred at room temperature for 4 h, and a white precipitate was obtained. Templates were extracted in acid ethanol solvent (15 mL of conc. HCl in 120 mL of ethanol) until no template could be detected by UV-Vis spectroscopy. Non-imprinted polymers (NIPs) were prepared *via* a similar process but without the template BPA.

Anchoring QDs into BPA-imprinted multilevel mesoporous silica

To prepare BPA-imprinted fluorescent polymers, carboxyl group-modified CdTe QDs were anchored on the BPA-imprinted multilevel mesoporous silica *via* a condensation reaction between the

carboxylic groups and amino groups, which was denoted as p-MIFPs. Briefly, 200 mg of BPA-imprinted multilevel mesoporous silica with amino groups was dispersed in 4 mL of water. The amino groups were activated by 2 mL of NHS (2 mg mL^{-1}) solution for 15 min. Then 1 mL of carboxyl group-modified CdTe QDs was added and stirred in the dark for 4 h. The obtained product was centrifuged and washed with ultrapure water for 3 times before drying under vacuum.

Construction of ratiometric fluorescent MIPs based on post-imprinting modification

Ratiometric fluorescent MIPs were also constructed using the post-imprinting modification strategy, which were denoted as p-r-MIFPs. Similarly to the above method, CDs and QDs were simultaneously bonded to the BPA-imprinted multilevel mesoporous silica.

Preparation of BPA-imprinted fluorescent polymer by one-pot doping method

BPA imprinted multilevel mesoporous fluorescent silica was also prepared *via* a one-pot doping method, which was denoted as d-MIFPs. Unlike the post-imprinting modification method, 1 mL of QDs was added to the polymerization system consisting of TEOS, APTES and BPA solvents. Considering that the fluorescence intensity of the QDs could be quenched obviously in the acid environment, the templates were washed with a mixture solvent of ethanol/acetonitrile (8 : 2). More time was needed than the acid-washing process.

BPA detection

The BPA detection was carried out as follows. Typically, a BPA standard solution was added to 4.0 mL of MIFPs or NIFPs probe solution with the final concentration of 1.0 nM to 50 μM. After incubation for 10 min, the fluorescence spectra were collected. For the p-MIFPs, the fluorescence intensity was measured under the following conditions: p-MIFPs or p-NIFPs 10 mg L^{-1}; reaction time 10 min, and the slit widths of emission and excitation were both 2.5 nm (n = 3). For the d-MIFPs, the fluorescence intensities were measured under the following conditions: d-MIFPs or d-NIFPs 50 mg L^{-1}; reaction time 10 min, and the slit widths of emission and excitation were both 5 nm (n = 3).

Real sample detection

To test the performance of the p-MIFPs in a complex matrix, river water samples were collected from the Yi River. The solid suspensions in the river water sample were filtered with a 0.22 μm membrane. Then the river water samples were spiked with BPA and recovery tests performed.

Results and discussion

Preparation of BPA-imprinted multilevel mesoporous fluorescent silica by post imprinting modification (p-MIFPs)

Generally, MIFPs were prepared by doping fluorescent nanoparticles into the polymerization solution, and fluorescent nanoparticles were coated inside the polymer during the polymerization process. During the preparation of MIFPs, the fluorescent nanoparticles undergo a polymer preparation process under alkaline conditions and template elution process under acidic conditions, and thus their fluorescence intensity is greatly reduced. In this work, BPA-imprinted fluorescent polymers were prepared by molecular imprinting and post-imprinting modification in two steps, as shown in Scheme 1. First, the MIPs were prepared by polymerization and template eluting in two steps. To facilitate the anchoring of the QDs into the MIPs, BPA-imprinted multilevel mesoporous silica was prepared. Small and large mesopores co-existed in the MIPs. The small mesopores may lead to increased surface area, and the large mesopores will allow the movement of nanoparticles in the porous matrices. Furthermore, the coexistence of multiple-scale pores may enhance and harmonize the diffusion of guest molecules. Multilevel mesoporous silica was prepared *via* the co-solvent method. Also, traditional mesoporous silica was prepared using CTAB as the soft template and water as the solvent. The mesopores were formed by the elution of the CTAB micelles. To form multilevel mesoporous silica, water, ethanol and ethyl ether were employed as co-solvents. The small mesopores were still formed by the elution of the CTAB micelles, while the large mesopores may be attributed to heterogeneous gasification of ethyl ether.[21] Then, the carboxyl group-modified CdTe QDs were anchored on the BPA-imprinted multilevel mesoporous silica by a condensation reaction between the carboxylic groups and amino groups. The QDs avoided the long polymerization and elution process, and the fluorescence intensity was maintained. It should be noted that for the post-imprinting modification method, the time required for the

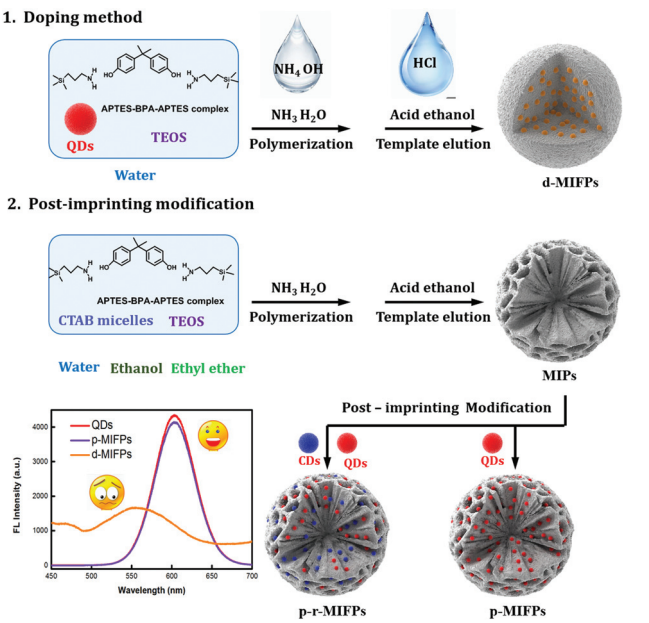

Scheme 1 Process for the preparation of MIFPs *via* the doping method and post-imprinting modification method.

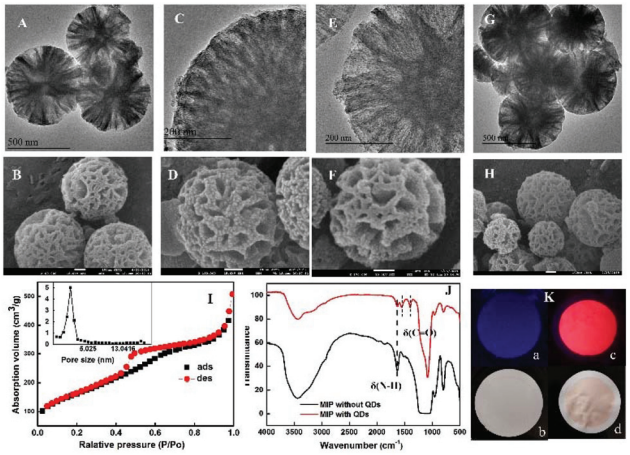

Fig. 1 TEM image of BPA-imprinted multilevel mesoporous silica (A and C), QD-anchored p-MIFPs (E) and p-NIFPs (G). Corresponding SEM images of BPA imprinted multilevel mesoporous silica (B and D), QD-anchored p-MIFPs (F) and p-NIFPs (H). N_2 sorption isotherms and the pore size distribution of p-MIPs (I). FTIR spectra of MIPs and p-MIFPs (J). Images of the MIPs before and after anchoring the QDs under UV light and sun light (K).

template elution is less and the template elution is more complete. Although the post-imprinting modification method is one step further than the doping method, its overall time is less than the doping method.

The TEM and SEM images confirmed the successful preparation of the multilevel mesoporous silica. As shown in Fig. 1A and B, the silica particles have a size of 500 nm, and their surface area was 588 $m^2\ g^{-1}$, as detected from the absorption and desorption isotherm. Large pores with a diameter of 10–60 nm can be observed from the TEM and SEM images and the wall thickness between the large holes was approximately 10–50 nm. The small mesopores can be observed in the HRTEM image, as shown in Fig. 1C, and also were confirmed by the nitrogen adsorption–desorption experiment (Fig. 1I). The diameter of the small mesopores was about 3.7 nm, as calculated from the adsorption branch of the isotherms.

The existence of amino groups in the multilevel mesoporous silica was confirmed by FT-IR. As shown in Fig. 1J, the typical bending vibration (δN–H) of the amino group at 1560 cm^{-1} can be observed. The amino groups were provided by APTES, and APTES has dual functions in this work. First, APTES acted as a functional monomer for BPA imprinting. Recognition sites were formed between the amino groups and template molecule. The other role of APTES was to anchor the QDs. Based on the condensation reaction between the carboxylic groups and amino groups, the QDs were anchored into the silica particles, and the TEM images (Fig. 1E) confirmed the successful anchoring of the QDs. The black dots uniformly dispersed inside the multilevel mesoporous silica observed from Fig. 1E are the anchored QDs. Fig. S1† provides the TEM images of the MIPs before and after anchoring the QDs with a big size and high definition. Meanwhile, the mapping of p-MIFPs verify the existence of CdTe QDs (Fig. S1†). Most QDs were anchored inside not on the surface of the silica particles, and thus the SEM images of the multilevel mesoporous silica before (Fig. 1D) and after (Fig. 1F) anchoring the QDs did not display obvious differences. The successful anchoring of the QDs was also verified by FT-IR and photos under UV light. The typical carboxylic group peaks (δ C=O) were observed from the QD-anchored silica. After anchoring the QDs, bright red fluorescence could be observed under 365 UV light (Fig. 1K). The morphology of the p-NIFPs (Fig. 1G and H) was similar to that of p-MIFPs, which indicated that the existence of the template did not affect the formation of the multilevel mesoporous silica.

Because APTES was used as a functional monomer for BPA imprinting, amino groups (NH_2) are the imprinting sites in the imprinting cavities. Then, does the introduction of QDs destroy the imprinting sites? The imprinting sites match the size, shape and functional groups of BPA, which are much smaller than that of QDs. It was difficult for the QDs with a big size to enter the imprinting sites of BPA, and thus the amino groups in the recognition site had limited chance to bind with the QDs. This inference was proven by the adsorption experiments. The effect of anchoring of QDs on the adsorption capacity of p-MIFPs was investigated by a static adsorption experiment and dynamic adsorption experiment according to the previously reported method,[22] and the results are displayed in Fig. S2.† The result showed that the anchored QDs did not affect the binding capacity and adsorption rate. This is mainly because the anchored QDs did not block the passage of the template molecules, and they did not occupy the recognition sites.

The fluorescence properties of the p-MIFPs were compared with that of d-MIFPs. First, the fluorescence intensity of MIFPs under ultraviolet light was compared, as shown in Fig. S3A–F.† The QDs displayed red color under a 365 nm ultraviolet lamp. However, d-MIFPs showed a weak yellow fluorescence under the 365 nm ultraviolet lamp. p-MIFPs displayed bright red fluorescence. Thus, to explore the reasons for the weakening of the fluorescence intensity and the change in the emission wavelength, a control experiment was performed using NIFPs. We found that the fluorescence intensity and emission wavelength changed during the polymerization process. The silicon spheres were prepared under alkaline conditions, which may have affected the electronic transition of the functional groups of the QDs. Thus, the fluorescence property the QDs changed under alkaline conditions. The fluorescence intensity of the QDs was further weakened after the long elution process. For the p-MIFPs, the QDs avoided the polymerization and elution process, and their fluorescence property was well kept. Thus, the post-imprinting modification method is advantageous for increasing the fluorescence intensity of MIFPs.

Then the fluorescence spectra of p-MIFPs and d-MIFPs were compared. As shown in Fig. S3G,† the maximum emission peak of d-MIFPs shifted from 600 nm to 550 nm. Meanwhile, the symmetry of the fluorescence spectra deteriorated. p-MIFPs retained the fluorescence properties of the QDs. Under the same concentration and detection conditions, the

fluorescence intensity of p-MIFP was significantly higher than that of d-MIFPs. We inferred and expected that the strategy of post-printing modification enjoyed the advantages of maintaining the fluorescence property of the QDs, reducing the detection background and improving the detection sensitivity.

Detection of BPA with p-MIFPs and d-MIFPs

To verify the strategy of post-imprinting modification in improving detection sensitivity, p-MIFPs and d-MIFPs were employed to detect BPA, and the sensitivity and detection limits of the two methods were compared. For the ideal detection results, the amount of p-MIFPs and d-MIFPs was optimized. The optimized concentration of p-MIFPs was 10 mg L^{-1} while it was 50 mg L^{-1} for d-MIFPs. Fig. 2 displays that the fluorescence intensity of the MIFPs gradually decreased with an increase in the concentration of BPA. For the p-MIFPs, the fluorescence quenching degree $(F_0 - F)/F_0$ at 600 nm was closely linear over the concentration of BPA ranging from 0.005–4.0 μM. The limit of detection for p-MIFPs was 0.57 nM, as calculated by the 3 times the standard deviation rule (3S/N). For the d-MIFPs, the fluorescence quenching degree $(F_0 - F)/F_0$ at 550 nm was closely linear over the concentration of BPA ranging from 2.0–40.0 μM with a limit of detection of 0.87 μM. The higher detection sensitivity of p-MIFPs is attributed to the following aspects, as compared in Table S1.† First, the optimized concentration of p-MIFPs (10 mg L^{-1}) is lower than that of d-MIFPs (50 mg L^{-1}), and a decrease in the concentration of d-MIFPs to 10 mg L^{-1} will result in a lower fluorescence intensity, which is hard to detect. Second, p-MIFPs displayed a good spectral performance and low detection background. Third, the functional groups on the surface of QDs in d-MIFPs would be destroyed and passivated during the polymerization and elution process. Fourth, the QDs was non-uniform distributed in the d-MIFPs, while the post-imprinting modification method ensured the uniform distribution of the QDs.[23]

To verify the selective recognition ability of MIFPs to BPA, the fluorescence spectra of NIFP to BPA were recorded, as shown Fig. 2B and D. The addition of BPA caused a slight decrease in the fluorescence intensity of p-NIFPs or d-NIFPs, displaying the lower sensitivity of NIFPs. The imprinting factors, defined as the ratio of the quenching constants (the slope of the standard curve) of the MIFPs and NIFPs, were calculated to be 15.7 and 3.2 for p-MIFPs and d-MIFPs, respectively. p-NIFPs and d-NIFPs both displayed lower sensitivity when detecting BPA, and the slope difference was relatively small. Thus, the higher imprinting factor of p-MIFPs is due to its higher detection sensitivity.

Stability and reusability of p-MIFPs

Stability, an important index for the proposed fluorescent sensor, was investigated and displayed in Fig. S4.† The fluorescence intensity of p-MIFPs was detected after storage at 4 °C for 30 days to verify its long-term stability. 93.2% of its original fluorescence intensity was retained, indicating the proposed p-MIFPs sensor has good storage stability. Furthermore, 91.5% of the original fluorescence intensity of p-MIFPs was retained after continuous excitation at 365 nm for 1 h, indicating its high photo-stability.

Reusability is a significant advantage of imprinted fluorescent sensors. After eluting the adsorbed BPA, p-MIFPs were re-used for a new round of BPA detection. As predicted, the fluorescence intensity of the QDs decreased after the elution process. After three cycles, the detection sensitivity was reduced by two orders of magnitude. The reusability of p-MIFPs will be improved in the following work.

Construction of molecular imprinted ratiometric fluorescent sensor based on post-imprinting modification (p-r-MIFPs)

Ratiometric fluorescent probes have the advantage of visual detection and are widely used in the field of molecular imprinting.[24,25] The role of the post-imprinting modification process in the construction of molecularly imprinted ratiometric fluorescent sensors was further examined. When both CDs and QDs were anchored on MIPs, ratiometric fluorescent MIPs were constructed. As expected, blue CDs and red QDs were simultaneously bonded to the multilevel mesoporous silica, and the molecular imprinted ratiometric fluorescent sensor was constructed, which was denoted as p-r-MIFPs. The morphology and fluorescence spectrum of p-r-MIFPs were characterized and displayed in Fig. S5.† p-r-MIFPs exhibited a similar morphology to p-MIFPs because of their same imprinting matrix. Similarly, the fluorescence spectrum properties of CDs and QDs were well-preserved in p-r-MIFPs.

By adjusting the amount of CDs and QDs, the ratio of the fluorescence intensity of the two emission peaks can be adjusted. This process is simple and easy to control. The ratio of the relative amounts of CDs and QDs was optimized to obtain the ideal sensitivity. When the amount of CDs was too low, the fluorescence intensity of the QDs had little effect on

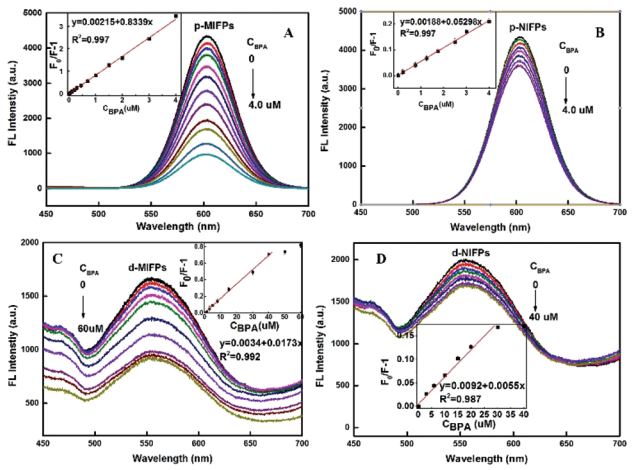

Fig. 2 Corresponding fluorescence spectra of p-MIPs (A), p-NIPs (B), d-MIPs (C), and d-NIPs (D) upon exposure to different concentrations of BPA. Insets show the plot of $(F_0/F - 1)$ as a function of BPA concentration. The experimental conditions were p-MIPs or p-NIPs 10 mg L^{-1}; silt widths of excitation and emission, 2.5 and 2.5 nm, respectively; d-MIPs or d-NIPs 50 mg L^{-1}; and silt widths of excitation and emission, 5.0 and 5.0 nm, respectively.

the fluorescence intensity of the CDs. With an increase in the concentration of BPA, the fluorescence intensity of the QDs decreased and the fluorescence intensity of the CDs remained unchanged, as can be seen from Fig. S6A.† The constructed ratiometric fluorescent probe tended to be a reference ratiometric fluorescent probe, which enjoyed a narrow colour range and low sensitivity.[26] When the amount of CDs was too high, the decrease in the fluorescence intensity of the QDs induced by BPA was compensated by the CDs because of the partial overlap of the fluorescence spectra of the CDs and QDs, which decreased the detection sensitivity, as displayed in Fig. S6B.† Considering the colour change and detection sensitivity, the initial intensity of the CDs was adjusted to be similar with that of the QDs, as displayed in Fig. 3A.

To evaluate the performance of p-r-MIFPs, the ratiometric fluorescence detection of BPA was performed. From Fig. 3 it can be seen that with the addition of BPA, the fluorescence intensity of the QDs decreased, while the fluorescence intensity of the CDs increased. The excitation spectrum of the QDs partially overlapped with the emission spectrum of the CDs (Fig. S6c†); thus, the increase in the fluorescence intensity of the CDs may be ascribe to the FRET between the CDs and QDs. (I445)/I605 was closely related to the amount of BPA ranging from 0.004 to 3.0 μM, with the detection limit as low as 0.13 nM. Visual detection of BPA was examined and the photos of the detection solution under 365 nm light are shown in Fig. 3A. With the addition of BPA, the colour of the p-r-MIFPs solution changed from pink to grey then to blue. A noticeable colour change could be observed throughout the process, and visual detection of BPA was feasible. In the meanwhile, the dose response of the p-r-NIFPs to BPA also was examined. From Fig. 3B, it can be seen that p-r-NIFPs displayed lower sensitivity than the corresponding p-r-MIFPs. Because the fluorescence intensity of the two peaks did not change much, the colour change of p-r-NIFPs was not distinguished. The results indicate that post-imprinting modification is an ideal strategy for the fabrication of molecularly imprinted ratiometric fluorescent polymers.

The stability and reusability of p-r-MIFPs were also investigated using the abovementioned methods, as shown in Fig. S7.† The proposed p-r-MIFPs also displayed good photo stability and storage stability. However, the reusability of p-r-MIFPs needs to be improved. It should be noted that even after three rounds of repeated use, the detection sensitivity of p-MIFPs was still in an order of magnitude higher than that of d-MIFPs.

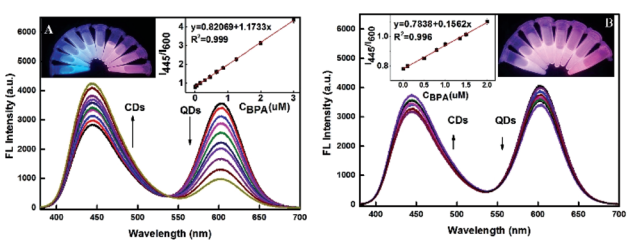

Fig. 3 Corresponding fluorescence spectra of p-r-MIFPs (A) and p-r-NIFPs (B) with different concentrations of BPA. Insets show the fluorescence colour of p-r-MIFPs and p-r-NIFPs in response to different concentrations of BPA under 365 nm UV light.

Selectivity of p-MIFPs

Selectivity is an important indicator of MIPs. An ideal MIP should exhibit specific recognition ability to template molecules, while not displaying a significant response to other molecules. Thus, the selectivity of p-MIFPs was demonstrated using template analogues (phenol, estradiol and cholesterol) and a metal ion (Hg^{2+}) as a control. As can be seen from Fig. 4A, p-MIFPs showed good selective recognition ability for BPA. BPA, phenol, estradiol and cholesterol have the same phenolic hydroxyl group, but they show great differences in their molecular structure and shape. Thus, this specific recognition ability stems from the differences in molecular size and shape. It well known that Hg^{2+} can quench QDs with high efficiency. However Hg^{2+} interference was eliminated by the molecular imprinting process because the BPA imprinted sites were not match to Hg^{2+} in terms of size, shape and coordinated functional groups. Using the same procedure, the selectivity of p-r-MIFPs was also measured. p-r-MIFPs also displayed good selectivity for BPA. Remarkable fluorescence color from pink to gray to blue was observed with the addition of BPA under UV light. In contrast, no obvious changes in fluorescence intensity ratio and color were seen after the addition of the control compounds. Thus, the selectivity experiments confirmed p-MIFPs had specific recognition ability toward BPA.

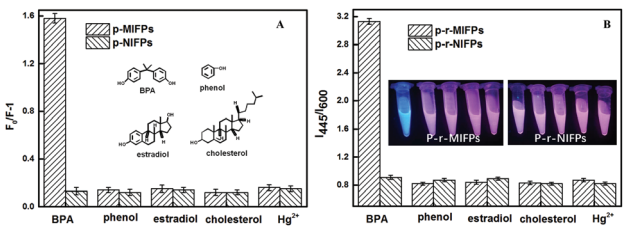

Fig. 4 Selectivity experiment for p-MIPs and p-r-MIFPs. The inset images show the fluorescence colours of p-r-MIFPs upon the addition of different targets with the concentration of 2 μM under 365 nm UV light.

Table 1 Spiked recoveries and RSDs (%, n = 3) for the determination of BPA in river water samples using p-MIFPs and p-r-MIFPs

Probe	Added (μM)	Found (μM)	Recovery (%)	RSD (%)
p-MIFPs	0	0	—	—
	0.100	0.097	97.0	3.2
	0.500	0.482	96.4	4.1
	2.000	2.012	100.6	3.7
p-r-MIFPs	0	0	—	—
	0.100	0.102	102	2.6
	0.500	0.494	98.8	3.1
	2.000	1.982	99.1	2.9

Table 2 Comparison of the construction strategy and sensing performance with the reported MIFPs for the detection of BPA

Sensor	Construction method	Emission mode	Linear range (μM)	LOD (nM)	Ref.
CdTe QDs@SiO_2	Doping	Single	0.05–10	6	27
AuNCs@SiO_2	Doping	Single	0–13.1	100	15
CDs-AuNCs@SiO_2	Doping	Dual	0.1–2.5	29	24
CDs@SiO_2	Doping	Single	0.1–4.2	30	28
SiO_2@CdTe QDs	Post modification	Single	0.005–4.0	0.57	This work
SiO_2@CdTe QDs & CDs	Post modification	Dual	0.004–3.0	0.13	This work

Detection of BPA in real samples

The measurement of BPA concentrations in water is important for evaluating compliance with water quality standards or environmental risk levels of this harmful compound in the environment. To evaluate the practical applicability of p-MIFPs, it was applied for the recovery analysis of BPA in spiked river water. The averaged recovery was obtained with relative standard deviation (RSD) based on three triplicate measure for each concentration. As listed in Table 1, satisfactory recoveries ranging from 96.4% to 100.6% with RSDs below 4.1% were obtained by p-MIFPs, and recoveries ranging from 98.8% to 102.0% with RSDs in the range of 2.6–3.1% by p-r-MIFPs. Thus, the results indicate that the post-imprinting modification is feasible for the synthesis of MIFPs.

Method performance comparison

The construction strategy and sensing performance of the developed p-MIFPs sensor for BPA detection were compared with that of the reported MIFPs. As listed in Table 2, a series of fluorescent nanoparticles, such as CdTe QDs,[27] AuNCs,[15] CDs,[28] and CDs-AuNCs dual emission nanoparticles[24] were embedded into imprinted silica particles *via* the doping method to provide BPA dosage-sensitive fluorescent sensors. In general, p-MIFPs achieved lower LODs compared with that of d-MIFPs, and the dual emission MIFPs achieved higher sensitivity compared with the single emission MIFPs. From Table 2, it can be seen that post-imprinting modification is an effective strategy to construct MIFPs.

Conclusions

In summary, a novel MIFPs sensor with outstanding sensitivity was successfully constructed *via* the post-imprinting modification strategy using multilevel mesoporous silica as the imprinting matrix. First, multilevel mesoporous silica was an ideal matrix for imprinting and post-imprinting modification. Its small mesopores lead to an increased surface area, and its large mesopores allowed the nanoparticles move into the porous matrices. Second, post-imprinting modification was an ideal strategy to construct MIFP with low background, high fluorescence intensity, uniform fluorescent nanoparticle distribution and highly active fluorescent nanoparticles. Specifically, this method is also suitable for the construction of p-r-MIFPs. As a successful proof-of-concept, we believe that the post-imprinting modification strategy can be further developed and applied for the construction of MIFPs, and variety of morphologies will be developed and suitable for post-imprinting modification.

Conflicts of interest

There are no conflicts to declare.

Acknowledgements

This work was supported by the National Natural Science Foundation of China (21777065) and the Taishan Scholar fund from Shandong Provence for financial support.

Notes and references

1 L. Chen, S. Xu and J. Li, *Chem. Soc. Rev.*, 2011, **40**, 2922–2942.
2 L. Chen, X. Wang, W. Lu, X. Wu and J. Li, *Chem. Soc. Rev.*, 2016, **45**, 2137–2211.
3 D. J. Li, Z. J. Bie, F. F. Wang and E. H. Guo, *Analyst*, 2018, **143**, 4936–4943.
4 D. J. Li, T. Y. Tu and X. Y. Wu, *Anal. Methods*, 2018, **10**, 4419–4429.
5 D. J. Li, T. Y. Tu, M. K. Yang and C. Xu, *Talanta*, 2018, **184**, 316–324.
6 D. J. Li, Q. Yuan, W. L. Yang, M. K. Yang, S. H. Li and T. Y. Tu, *Anal. Biochem.*, 2018, **561–562**, 18–26.
7 H. Zhu, J. Fan, B. Wang and X. Peng, *Chem. Soc. Rev.*, 2015, **44**, 4337–4366.
8 L. Zhang and L. Chen, *ACS Appl. Mater. Interfaces*, 2016, **8**, 16248–16256.
9 D. J. Li, N. Wang, F. F. Wang and Q. Zhao, *Anal. Methods*, 2019, **11**, 3212–3220.
10 H. Lu, C. Yu and S. Xu, *Sens. Actuators, B*, 2019, **288**, 691–698.
11 Q. Yang, J. Li, X. Wang, H. Xiong and L. Chen, *Anal. Chem.*, 2019, **91**(10), 6561–6568.
12 Q. Yang, J. Li, X. Wang, H. Peng, H. Xiong and L. Chen, *Biosens. Bioelectron.*, 2018, **112**, 54–71.
13 S. Huang, M. Guo, J. Tan, Y. Geng, J. Wu, Y. Tang, C. Su, C. Lin and Y. Liang, *ACS Appl. Mater. Interfaces*, 2018, **10**, 39056–39063.
14 B. Demir, M. M. Lemberger, M. Panagiotopoulou, P. X. M. Rangel, S. Timur, T. Hirsch, B. T. S. Bui, J. Wegener and K. Haupt, *ACS Appl. Mater. Interfaces*, 2018, **10**, 3305–3313.

15 X. Wu, Z. Zhang, J. Li, H. You, Y. Li and L. Chen, *Sens. Actuators, B*, 2015, **211**, 507–514.
16 R. C. Stringer, S. Gangopadhyay and S. A. Grant, *Anal. Chem.*, 2010, **82**, 4015–4019.
17 Y. Miao, X. Sun, J. Lv and G. Yan, *ACS Appl. Mater. Interfaces*, 2019, **11**, 2264–2272.
18 X. Du and J. He, *Nanoscale*, 2011, **3**, 3984–4002.
19 H. Lu, S. Quan and S. Xu, *J. Agric. Food Chem.*, 2017, **65**, 9807–9814.
20 S. Zhu, Q. Meng, L. Wang, J. Zhang, Y. Song, H. Jin, K. Zhang, H. Sun, H. Wang and B. Yang, *Angew. Chem., Int. Ed.*, 2013, **52**, 3953–3957.
21 X. Du and J. He, *Langmuir*, 2010, **26**, 10057–10062.
22 S. Xu, J. Li and L. Chen, *Talanta*, 2011, **85**, 282–289.
23 D. Li, X. He, Y. Chen, W. Li and Y. Zhang, *ACS Appl. Mater. Interfaces*, 2013, **5**, 12609–12616.
24 H. Lu and S. Xu, *Biosens. Bioelectron.*, 2017, **92**, 147–153.
25 S. Xu and H. Lu, *Chem. Commun.*, 2015, **51**, 3200–3203.
26 H. Lu, C. W. Yu, S. Quan and S. Xu, *Analyst*, 2019, **144**, 1153–1158.
27 C. Qiu, Y. Xing, W. Yang, Z. Zhou, Y. Wang, H. Liu and W. Xu, *Appl. Surf. Sci.*, 2015, **345**, 405–417.
28 G. Liu, Z. Chen, X. Jiang, D. Feng, J. Zhao, D. Fan and W. Wang, *Sens. Actuators, B*, 2016, **228**, 302–307.